Influence of Surface Waviness of Journal and Bearing Bush on the Static Characteristics of Hydrodynamic Bearing

Authors:

Minghui Yang, Hong Lu, Xinbao Zhang, Meng Duan, Liu Bao, Bowen Wang, Wan Wu

Date Submitted: 2022-01-24

Keywords: hydrodynamic journal bearing, surface waviness, finite difference method, static characteristics

Abstract:

An investigation on the surface waviness of both the journal and the bearing bush and their impact on the static characteristics of the hydrodynamic journal bearing is presented in this paper. The finite difference method is introduced to solve a Reynolds equation and obtain the unknown pressure field. The static characteristics, including the load carrying capacity, attitude angle, end leakage flow rate and frictional coefficient are studied under different waviness parameters. The numerically simulated results indicate that the waviness of the bearing bush may deteriorate or enhance the bearing system, depending on the phase angle. The waviness of the journal causes periodic changes in bearing behavior, owing to the alteration in the phase angle. The profile of the journal and bearing surfaces near the attitude angle determines the performance of the bearing system.

DOI of Published Version: https://doi.org/10.3390/pr9010110 processes

Article

Influence of Surface Waviness of Journal and Bearing Bush on the Static Characteristics of Hydrodynamic Bearing

Minghui Yang [1], Hong Lu [1], Xinbao Zhang [2,*], Meng Duan [1], Liu Bao [1], Bowen Wang [1] and Wan Wu [1]

[1] School of Mechanical and Electronic Engineering, Wuhan University of Technology, Wuhan 430070, China; yangminghui@whut.edu.cn (M.Y.); landzh@whut.edu.cn (H.L.); duanmeng@whut.edu.cn (M.D.); baoliu@whut.edu.cn (L.B.); wangbowen1026@whut.edu.cn (B.W.); 1542112315003@whut.edu.cn (W.W.)
[2] School of Mechanical Science and Engineering, Huazhong University of Science and Technology, Wuhan 430070, China
* Correspondence: zhangxinbao1@hust.edu.cn

Abstract: An investigation on the surface waviness of both the journal and the bearing bush and their impact on the static characteristics of the hydrodynamic journal bearing is presented in this paper. The finite difference method is introduced to solve a Reynolds equation and obtain the unknown pressure field. The static characteristics, including the load carrying capacity, attitude angle, end leakage flow rate and frictional coefficient are studied under different waviness parameters. The numerically simulated results indicate that the waviness of the bearing bush may deteriorate or enhance the bearing system, depending on the phase angle. The waviness of the journal causes periodic changes in bearing behavior, owing to the alteration in the phase angle. The profile of the journal and bearing surfaces near the attitude angle determines the performance of the bearing system.

Keywords: hydrodynamic journal bearing; surface waviness; finite difference method; static characteristics

check for updates

Citation: Yang, M.; Lu, H.; Zhang, X.; Duan, M.; Bao, L.; Wang, B.; Wu, W. Influence of Surface Waviness of Journal and Bearing Bush on the Static Characteristics of Hydrodynamic Bearing. *Processes* **2021**, *9*, 110. https://doi.org/10.3390/pr9010110

Received: 27 November 2020
Accepted: 4 January 2021
Published: 7 January 2021

1. Introduction

Journal bearings have been widely used in the industry because of their advantages of a low friction and high load capacity, as well as noise and vibration reduction. In engineering practices, it is impossible to manufacture perfect machine components, although highly precise, accurate processing methods and equipment are available nowadays. Likewise, surface waviness may occur during the manufacturing processes of journals and bearing bushes. The effect of the shape errors of the journal and the bearing bush on the performance of the bearing system is quite significant, since this determines the gap geometry and hence the pressure generated.

A number of researchers focused their attention on examining the effect of a journal's shape errors on the characteristics of the bearing system, and lots of achievements have been made [1–8]. Wilson [1] carried out an experiment to study the effect of a journal's geometry imperfections on hydrodynamic bearing performance characteristics. Mokhtar et al. [2,3] theoretically and experimentally investigated the effect of the surface waviness parameters of a journal on the static characteristics of hydrodynamic bearings. Chennabasavan and Raman [4] examined the influence of a journal's irregularities on the performance of porous hydrodynamic bearings. Recently, the effect of a journal's geometric irregularities, such as in the barrel shape, bellmouth shape, circumferential undulations and the ideal shape, on a hydrostatic bearing was studied in combination with the influence of a micropolar lubricant [5], the influence of different pocket geometries [6], the influence of a non-circular journal bearing [7], and the influence of a misaligned journal [8]. The studies [1–8] indicated that the journal's geometric irregularities have a great contribution to altering the bearing performance. Therefore, more investigations need to be carried out to reveal the effect of a journal's geometrical irregularities on the bearing performance characteristics. However, as noted above, the studies were limited to a journal's irregularities and neglected the effect of waviness on the bearing.

In a practical situation, due to the limitations of processing equipment and processing methods, surface waviness on the bearing bush cannot be eliminated completely. A number of studies [9–18] examined the effect of bearing imperfections on the characteristics of various bearing systems. Dimofte [9,10] evaluated the performance of a three-wave journal bearing and revealed that the wave's amplitude and position had a significant influence on the bearing's characteristics. Lin [11,12] examined the influence of the width and height of the three-dimensional asperities on bearing performance in a steady state. Ostayen et al. [13] analyzed the influence of the random track surface waviness on the load capacity and flow rate of the thrust bearing. Kwan and Post [14] demonstrated the sensitivity of the bearing's load capacity and stiffness to manufacturing errors. Rahmatabadi et al. [15] revealed that the static performance characteristics of a lobed bearing were influenced by the bearing configurations. Furthermore, the effect of the presence of surface waviness of the bearing bush in the circumferential and axial direction [16–18] on the bearing system were analyzed. Zmarzly [19] showed the effect of radial clearance values on the vibration level of a bearing system. However, the above studies mainly focused on the effect of the bearing's shape on bearing performances, and the effect of the journal's shape was neglected.

In recent years, certain literature investigated the influence of wear [20–23] and surface roughness [24,25] on the behavior of a bearing system, and these studies indicated that the surface morphology substantially affects the performance of journal bearing systems. Some studies [26,27] analyzed the performance of the journal bearing with a partial surface texture and revealed that the surface texture parameters and texture distribution have an obvious influence on the behavior of bearing systems.

The bearing clearance, which is influenced by the surface shape of both the journal and the bearing bush, significantly contributes to affecting the performance of a bearing system. Hence, to improve the design of journal bearings with more accurately predicted data, the surface profile of both the journal and the bearing should be taken into consideration simultaneously. Jain and Sharma [28,29] revealed that the non-circularity of the bearing's and journal's geometric imperfections significantly affect the performance of a bearing system. Cui et al. [30,31] studied the influence of manufacturing errors on the static characteristics of aerostatic porous journal bearings, and the numerical and experimental results demonstrated that the bearing behavior was greatly affected by the wave amplitude and spatial wavelength. Zoupas et al. [32] showed that manufacturing errors can greatly affect the bearing performance. It was found that the investigation of the surface shape of both the journal and the bearing bush and their effects on the bearing characteristics was not sufficient.

As can be seen from the previous references, the geometric imperfections of journals and bearing bushes significantly affect the performance of the bearing system. However, to the author′s knowledge, there are not comprehensive studies considering the effects of both the surface waviness of the journal and the bearing bush on the performance of the hydrodynamic journal bearing. It is the aim of this paper to fill this gap. The numerical modeling studies the effect of the phase angle, amplitude and wavelength of the surface waviness of the journal and the bearing bush on the static performance of hydrodynamic journal bearings.

2. Theoretical Analysis

The Reynolds equation was derived from the Navier–Stokes equations, and the following assumptions were made. The laminar lubricant was isoviscous and incompressible and neglected the external force and the inertia force. Meanwhile, a no-slip boundary was used, and the velocity gradient was ignored except in the circumferential and axial directions. In the condition of the presence of surface waviness of the journal and the bearing bush, the oil film thickness was very small compared with the bearing length and the width of the bearing. Therefore, the Navier–Stokes equations reduce to the Reynolds equation.

For the journal bearings, the squeeze effects and the assumption that the bearing was in a steady state are neglected. The Reynolds equation can be expressed as the following form [2,4,11–13,15–18]:

$$\frac{\partial}{\partial X}\left(h^3\frac{\partial p}{\partial X}\right)+\frac{\partial}{\partial Z}\left(h^3\frac{\partial p}{\partial Z}\right)=6\eta U\frac{\partial h}{\partial X} \tag{1}$$

where η is the dynamic viscosity of the oil, X, Z are the Cartesian coordinates, h is the oil film thickness, p is the oil film pressure and U is the velocity of the oil on the journal's surface.

Let us use the dimensionless parameters

$$\phi=\frac{X}{r},\lambda=\frac{Z}{L/2},\overline{H}=h/c,\overline{p}=\frac{p}{6U\eta r/c^2} \tag{2}$$

The dimensionless Reynolds equation can be expressed as

$$\frac{\partial}{\partial \phi}\left(\overline{H}^3\frac{\partial \overline{P}}{\partial \phi}\right)+\frac{D^2}{L^2}\frac{\partial}{\partial \lambda}\left(\overline{H}^3\frac{\partial \overline{P}}{\partial \lambda}\right)=\frac{\partial \overline{H}}{\partial \phi} \tag{3}$$

where L is the axial length of the bearing, D is the diameter of the bearing, c is the bearing clearance, $\overline{H}$ is the dimensionless oil film thickness, $\overline{P}$ is the dimensionless oil film pressure and ϕ and λ are the dimensionless Cartesian coordinates.

The influence of the surface waviness of the journal and the bearing bush on bearing performance is mathematically modeled in the expression of the oil film thickness.

2.1. Oil Film Thickness

The journal bearing geometry configuration with surface waviness both on the journal and the bearing bush is shown in Figure 1. The dimensionless oil film thickness is expressed as follows:

$$\overline{H}=1+\varepsilon\cos\phi+\overline{H}_1+\overline{H}_2 \tag{4}$$

where $\overline{H}_1$ indicates the change in the dimensionless oil film thickness due to the surface waviness of the journal, $\overline{H}_2$ indicates the change in the dimensionless oil film thickness due to the surface waviness of the bearing bush and ε is the eccentricity ratio.

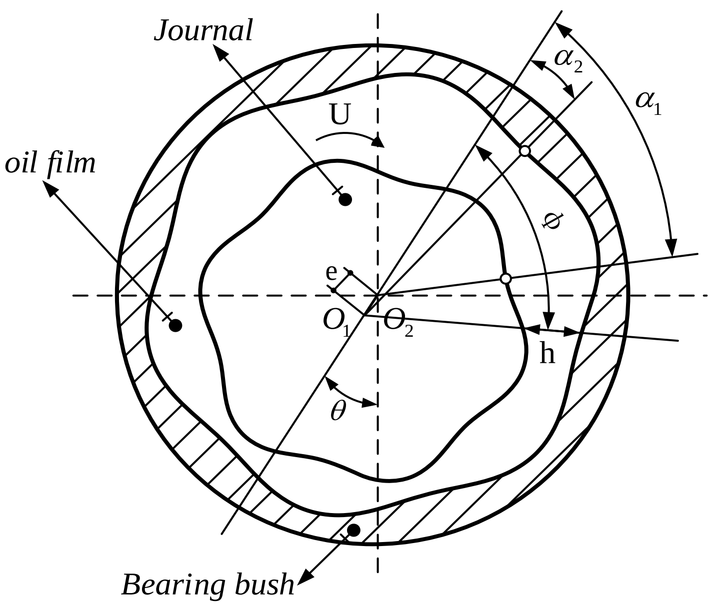

Figure 1. Illustration of the journal bearing with surface waviness.

The effect of the surface waviness of the journal on the fluid film profile is expressed as follows:

$$\overline{H}_1 = A_1 \cos[n_1(\phi - \alpha_1)] \tag{5}$$

The effect of the surface waviness of the bearing bush on the fluid film profile is expressed as follows:

$$\overline{H}_2 = -A_2 \cos[n_2(\phi - \alpha_2)] \tag{6}$$

where n_1 and n_2 are the number of waves of the journal and the bearing bush, α_1,α_2 is the angle between the wave trough and the attitude angle (θ), as shown in Figure 1, ϕ is the angular coordinate starting from the attitude angle, and A_1 and A_2 are the journal and bearing bush surface waviness amplitude ratios.

2.2. Finite Difference Method

The finite difference method was adopted to solve the Reynolds equation and gain the film pressure distribution. First, the film in the bearing system is unfolded into a plane from the attitude angle, and then the plane is equally meshed in the circumferential and axial directions. The partial derivatives in the Reynolds equation can be represented by the difference quotient of the pressure at each grid point, and the equations are transformed into a set of algebraic equations. Then, according to the boundary conditions, the pressure value at each node is iteratively obtained. By integrating the pressure value of the oil film, the bearing capacity can be obtained, and then the other lubricating properties of the bearing can be analyzed.

The partial derivatives in Equation (2) on each grid point (*i*,*j*) can be expressed as

$$\begin{aligned} \frac{\partial}{\partial\phi}\left(\overline{H}^3\frac{\partial\overline{p}}{\partial\phi}\right) &= \frac{\left(\overline{H}^3\frac{\partial\overline{p}}{\partial\phi}\right)_{i+1/2,j}-\left(\overline{H}^3\frac{\partial\overline{p}}{\partial\phi}\right)_{i-1/2,j}}{\Delta\phi} \\ &= \overline{H}^3_{i+1/2,j}\frac{\overline{p}_{i+1,j}-\overline{p}_{i,j}}{(\Delta\phi)^2} - \overline{H}^3_{i-1/2,j}\frac{\overline{p}_{i,j}-\overline{p}_{i-1,j}}{(\Delta\phi)^2} \end{aligned} \tag{7}$$

$$\begin{aligned} \frac{\partial}{\partial\lambda}\left(\overline{H}^3\frac{\partial\overline{p}}{\partial\lambda}\right) &= \frac{\left(\overline{H}^3\frac{\partial\overline{p}}{\partial\lambda}\right)_{i,j+1/2}-\left(\overline{H}^3\frac{\partial\overline{p}}{\partial\lambda}\right)_{i,j-1/2}}{\Delta\lambda} \\ &= \overline{H}^3_{i,j+1/2}\frac{\overline{p}_{i,j+1}-\overline{p}_{i,j}}{(\Delta\lambda)^2} - \overline{H}^3_{i,j-1/2}\frac{\overline{p}_{i,j}-\overline{p}_{i,j-1}}{(\Delta\lambda)^2} \end{aligned} \tag{8}$$

Then, the following matrices can be obtained:

$$A_{i,j}\overline{P}_{i+1,j} + B_{i,j}\overline{P}_{i-1,j} + C_{i,j}\overline{P}_{i,j+1} + D_{i,j}\overline{P}_{i,j-1} + E_{i,j}\overline{P}_{i,j} = F_{i,j} \tag{9}$$

where

$$A_{i,j} = \overline{H}^3_{i+1/2,j} \tag{10}$$

$$B_{i,j} = \overline{H}^3_{i-1/2,j} \tag{11}$$

$$C_{i,j} = (\frac{D}{L}\frac{\Delta\phi}{\Delta\lambda})^2\overline{H}^3_{i,j+1/2} \tag{12}$$

$$D_{i,j} = (\frac{D}{L}\frac{\Delta\phi}{\Delta\lambda})^2\overline{H}^3_{i,j-1/2} \tag{13}$$

$$E_{i,j} = A_{i,j} + B_{i,j} + C_{i,j} + D_{i,j} \tag{14}$$

$$F_{i,j} = \Delta\phi(\overline{H}_{i+1/2,j} - \overline{H}_{i-1/2,j}) \tag{15}$$

The dimensionless film pressure $\overline{P}_{i,j}$ is expressed as

$$\overline{P}_{i,j} = \frac{A_{i,j}\overline{P}_{i+1,j} + B_{i,j}\overline{P}_{i-1,j} + C_{i,j}\overline{P}_{i,j+1} + D_{i,j}\overline{P}_{i,j-1} - F_{i,j}}{E_{i,j}} \tag{16}$$

where $A_{i,j}$, $B_{i,j}$, $C_{i,j}$, $D_{i,j}$, $E_{i,j}$ and $F_{i,j}$ are coefficient matrices.

2.3. Boundary Conditions

The following boundary conditions are adopted to solve Equation (3):

$$\overline{P}(\phi, \lambda = \pm 1) = 0 \tag{17}$$

$$\overline{P}(\phi_1, \lambda) = 0 \tag{18}$$

$$\overline{P}(\phi_2, \lambda) = \partial \overline{P}(\phi_2, \lambda)/\partial \phi = 0 \tag{19}$$

where ϕ_1 and ϕ_2 are the angles of the start and end points of a hydrodynamic film for each axial plane.

2.4. Static Characteristics Parameters

2.4.1. Dimensionless Load Capacity and Attitude Angle

The dimensionless load carrying capacity of the bearing can be established by using the force balance. The dimensionless load components at x and z coordinates are expressed as

$$\overline{F}_z = -\int_{-1}^{1} \int_{0}^{2\pi} \overline{P} \cos(\theta + \phi) d\phi d\lambda \tag{20}$$

$$\overline{F}_x = -\int_{-1}^{1} \int_{0}^{2\pi} \overline{P} \sin(\theta + \phi) d\phi d\lambda \tag{21}$$

And the attitude angle θ can be expressed by an iterative solution until the convergence criterion is satisfied:

$$\frac{\overline{F}_x}{\overline{F}_z}| \leq 10^{-5} \tag{22}$$

The total dimensionless load capacity is

$$\overline{F} = \overline{F}_z \tag{23}$$

2.4.2. Dimensionless End Leakage Flow Rate

The dimensionless leakage flow rate from both ends of the plane of the bearing can be represented by the following formula:

$$\overline{Q}_1 = -\int_{0}^{2\pi} \overline{H}^3 * \frac{\partial \overline{p}}{\partial \lambda}|_{\lambda=1} d\phi \tag{24}$$

$$\overline{Q}_2 = -\int_{0}^{2\pi} \overline{H}^3 * \frac{\partial \overline{p}}{\partial \lambda}|_{\lambda=-1} d\phi \tag{25}$$

The total dimensionless end leakage flow rate of the lubricant is expressed as

$$\overline{Q} = \overline{Q}_1 + \overline{Q}_2 \tag{26}$$

2.4.3. Frictional Coefficient

The circumferential frictional force on the journal surface can be calculated as

$$F_c = -\int_{0}^{L} \int_{0}^{2\pi R} (\frac{\mathrm{h}}{2} \frac{\partial p}{\partial x} + \eta \frac{U}{h}) dx dz \tag{27}$$

Then, the circumferential friction coefficient is expressed as

$$\mu = \frac{F_c}{F} \tag{28}$$

3. Solution Procedure

Figure 2 describes the flow chart illustrating the solution procedure used in this study. Initially the bearing parameters, the number of grids, the eccentricity ratio ε and the tentative values of the attitude angle were input into the program. The governing equation (Equation (3)) was solved, along with the oil film thickness equations and boundary conditions defined in the earlier sections. The Gauss–Seidel method is adopted to obtain film pressure distribution, and the iterative process will continue until the convergence, as shown in Equation (29), is attained. k is the number of iterations in Equation (29). During the entire process of the iterative calculation, the cavitation effect is considered by setting all negative pressures to zero. The Newton–Raphson method is used to obtain the attitude angle. The inner loop is used to ensure the convergence of the pressure distribution, while the outside loop guarantees the convergence of the attitude angle. The iteration is repeated until the required tolerance is satisfied, as indicated in Figure 2:

$$\frac{\sum\limits_{i=1}^{m}\sum\limits_{j=1}^{n}\left|P_{i,j}^{k+1}-P_{i,j}^{k}\right|}{\sum\limits_{i=1}^{m}\sum\limits_{j=1}^{n}\left|P_{i,j}^{k+1}\right|}=Err_p \tag{29}$$

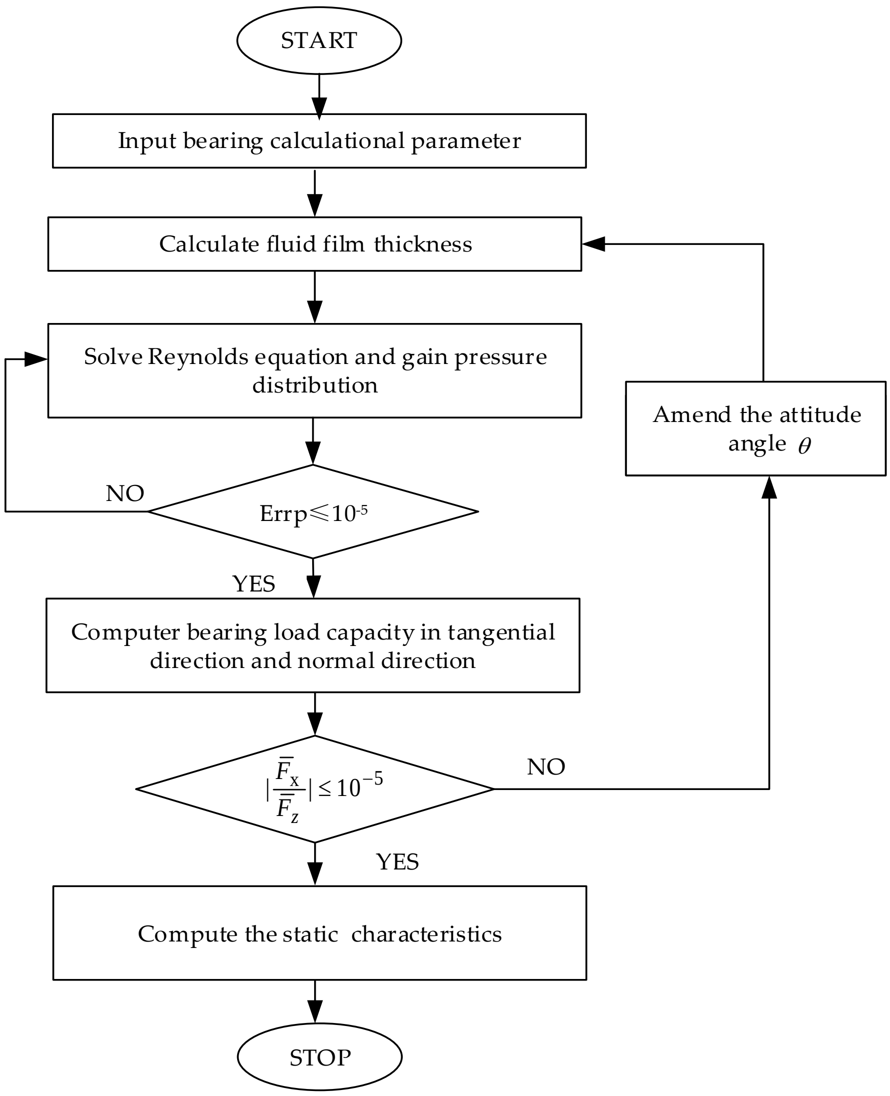

Figure 2. A flow chart to illustrate the solution procedure.

For a vertical external load $\overline{w}$, due to the presence of surface waviness on the journal and bearing bush, the corresponding journal center equilibrium position ($\varepsilon\theta$) is not unique. Therefore, it is difficult to illustrate the variation of the equilibrium position with the external load. In this paper, the static characteristics of the bearing system were studied under different eccentricity ratios.

4. Results and Discussion

To simulate the static characteristics of the hydrodynamic journal bearing, a model was developed according to theoretical analysis and the solution procedure discussed in the earlier section. In order to confirm the accuracy of the developed model, the simulated results of the hydrodynamic journal bearings with no surface waviness on the journal and the bearing bush from this model were compared with those found in [33]. Figure 3 shows the comparison of the load capacity, altitude angle, circumferential friction coefficient and dimensionless end leakage flow rate against the eccentricity ratio from this paper and in [33]. It can be seen that the results of the hydrodynamic journal bearings from the present work are in good agreement with those found in [33], which indicates the validation of the numerical model proposed in this study.

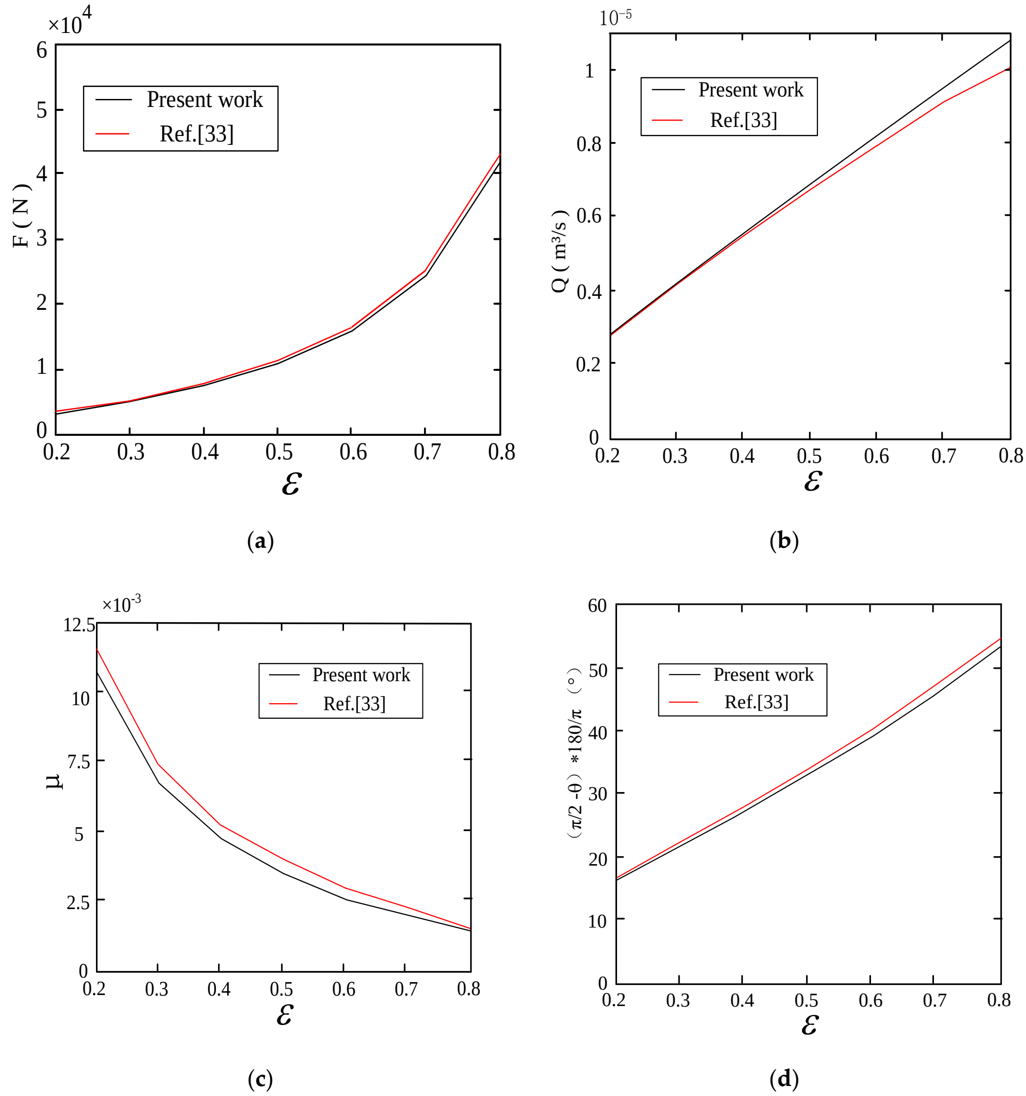

Figure 3. Comparison of the load carrying capacity (**a**), end leakage flow rate (**b**), frictional coefficient (**c**) and attitude angle (**d**) from [33] and the present analysis.

The bearing parameters and lubricant properties from the published paper are listed in Table 1. The dimensionless bearing geometric parameters and the surface waviness parameters of the present study are listed in Table 2.

Table 1. Bearing parameters and lubricant properties from [33].

Parameters.	**Value**
Journal radius	30 mm
Bearing length	66 mm
Radial clearance	0.03 mm
Rotational speed	3000 r/min
Lubricant viscosity	0.009 pa s

Table 2. Dimensionless bearing′s parameters of the present study.

Parameters	**Value**
r: Journal radius	30 mm
L: Bearing length	60 mm
c: Radial clearance	0.03 mm
n: Rotational speed	3000 r/min
g: Lubricant viscosity	0.0125 pa s
n_1: Waviness number of journal	3, 6, 9
n_2: Waviness number of bearing bush	3, 6, 9
A_{m1}: Waviness amplitude of journal	(1.2, 1.5, 1.8) μm
A_1: Waviness amplitude ratio of journal (A_{m1}/c)	0.04, 0.05, 0.06
A_{m2}: Waviness amplitude of bearing bush	(2.4, 3.0, 3.6) μm
A_2: Waviness amplitude ratio of bearing bush (A_{m2}/c)	0.08, 0.1, 0.12
α_1: Waviness phase angle of journal	$[0–360/n_1]$
α_2: Waviness phase angle of bearing bush	$[0–360/n_2]$

4.1. With Surface Waviness Only on the Journal or the Bearing Bush

The analysis for the effect of the surface waviness of the journal or the bearing bush was conducted to compare the results with the ideal shaft and bearing bush. Figures 4 and 5 show the effect of the phase angles of the surface waviness of the journal α_1 or bearing bush α_2 on bearing performance. The eccentricity ratio was 0.5. Due to the manufacturing precision of the journal being higher in practice than that of the bearing bush, the wave amplitude ratio of the journal was assumed to be 0.05 and the bearing bush was assumed to be 0.1. α_1 and α_2 had the opposite effect on the bearing performance, as can be seen from Figures 4 and 5. This is expected since the surface waviness of the journal and the bearing bush had the opposite effect on the bearing clearance, as can be seen from Equations (5) and (6). The bearing clearance changed the pressure distribution and then affected the bearing performance. The variation of the bearing performance with phase angles presented cosine curves, and the curve amplitude of the bearing bush was bigger than that of the journal. This is because the amplitude of the surface waviness of the bearing bush was greater than that of the journal, and the variation of clearance caused by the bearing bush was greater than that of the journal. Furthermore, in cases where only the bearing bush had surface waviness, the values of $\overline{F}$, $\overline{Q}$, μ and θ could be represented with cosine curves with periods of $360/n_2$.

As can be seen from Figure 4a, near the phase angles $\alpha_2 = 0$ and $\alpha_1 = 60°$, $\overline{F}$ gets its minimum value, while Figure 5a shows that there existed phase angles $\alpha_2 = 30°$ and $\alpha_1 = 0$, approximately at which $\overline{F}$ took its minimum value. This is probably due to the pressure near the attitude angle having a great contribution to the load capacity of the bearing. When $\overline{F}$ reached its minimum value, the film thickness caused by the waviness of the journal and the bearing bush was at its maximum near the attitude angle, and the pressure generated by the film reached its minimum. Figure 6 shows the phase angles of the bearing bush and the journal, corresponding to the minimum value of $\overline{F}$, and the value of oil film reaching its maximum.

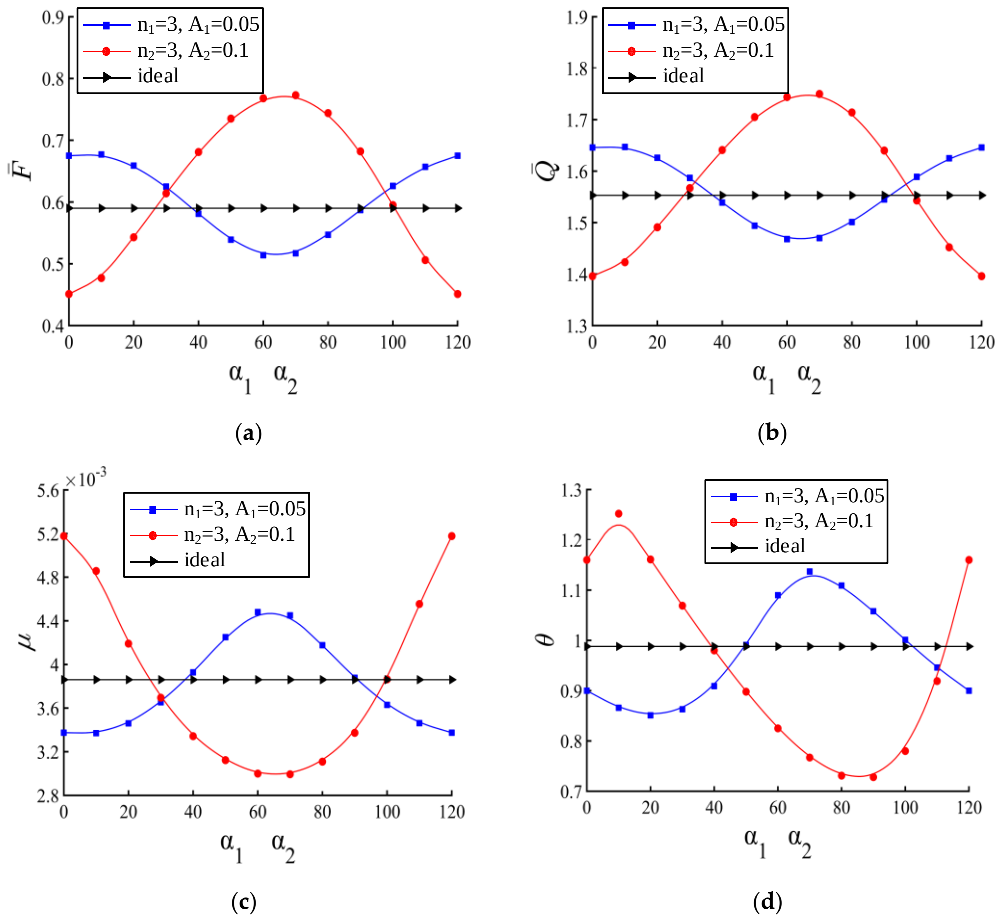

Figure 4. Variations of the dimensionless bearing load capacity (**a**), dimensionless end leakage flow rate (**b**), friction coefficient (**c**) and altitude angle (**d**) with phase angles of $A_1 = 0.05$, $A_2 = 0.1$ and $n_1 = n_2 = 3$.

4.2. *Effect of the Combined Waviness Phase Angle*

In this section, the effect of the waviness phase angle of both the journal and the bearing bush on the performance of the bearing were studied for four cases, namely (n_1= 3,n_2= 3), (n_1= 3,n_2= 6), (n_1= 6,n_2= 3) and (n_1= 6,n_2= 6), and the eccentricity ratio was 0.5. The wave amplitude ratio of the journal was 0.05, and for the bearing bush it was 0.1. The variation range of the waviness phase angle of the journal was from 0 to 360°/n_1, and for the bearing bush it was from 0 to 360°/n_2.

4.2.1. Influence on Dimensionless Load Capacity

Figure 7 shows the dimensionless bearing load capacity $\overline{F}$ against the phase angles of the surface waviness both on the journal α_1 and the bearing bush α_2 under four cases. The noticeable observation from Figure 7a,c is that the value of $\overline{F}$ first increased and then decreased with the change of α_2 from 0° to 120°, and it reached its maximum at approximately α_2= 60°, which coincides with the changing trend of Figure 4a in the case of $n_2 = 3$. Similarly, the value of $\overline{F}$ in Figure 7b,d first decreased and then increased with the change of α_2 from 0° to 60°, and it reached its maximum at approximately α_2= 0°, which is similar to the changing trend in Figure 5a in the case of $n_2 = 6$. The above change trends of $\overline{F}$ were expected, since for any phase angle α_1, the change trends of the film thickness caused by α_2 is similar with the situation of surface waviness only on the bearing, and vice versa. Therefore, the change trends of $\overline{F}$ in the combined waviness condition against

α_2 were similar with the condition of surface waviness only on the bearing. Furthermore, it can be observed from Figure 7 that the maximum pressure in the combined condition was greater than either of the corresponding conditions. This is mainly due to the fact that, in the combined surface waviness condition, the oil film was further reduced, and the maximum pressure and $\overline{F}$ increased.

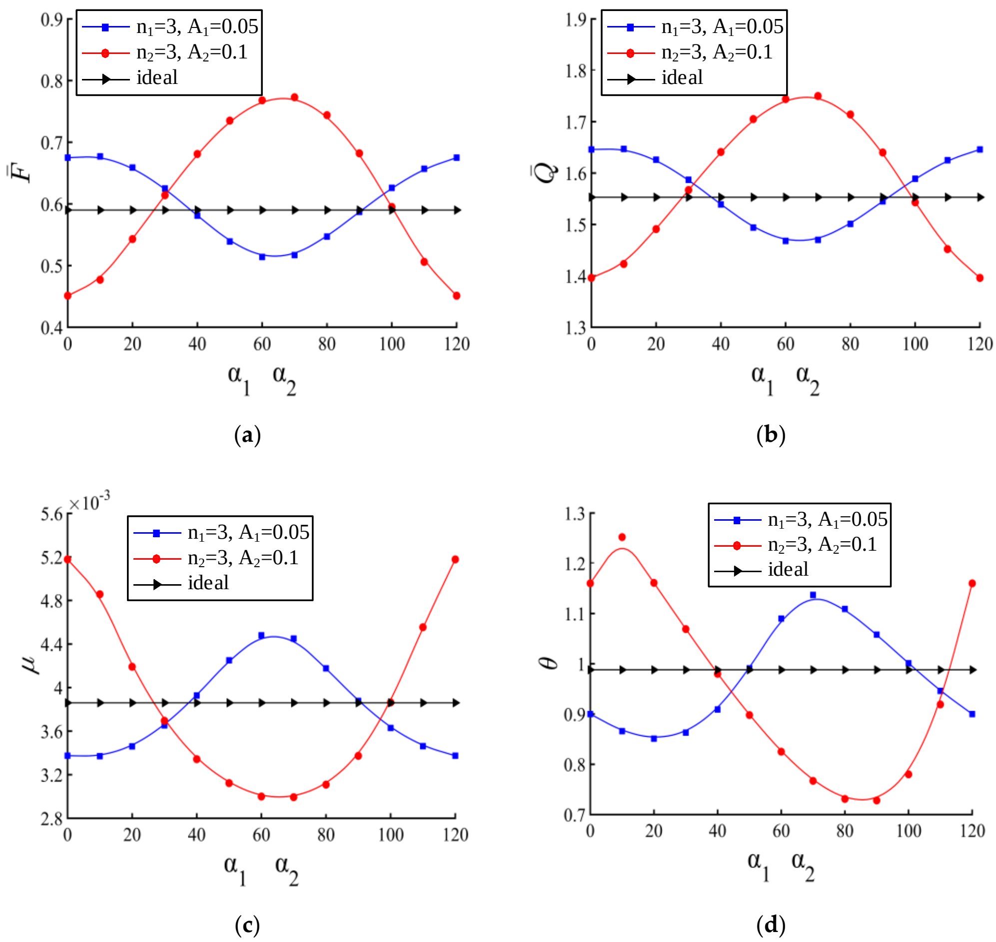

Figure 5. Variations of the dimensionless bearing load capacity (**a**), dimensionless end leakage flow rate (**b**), friction coefficient (**c**) and altitude angle (**d**) with phase angles of $A_1 = 0.05$, $A_2 = 0.1$ and $n_1 = n_2 = 6$.

4.2.2. Influence on Dimensionless End Leakage Flow Rate

The dimensionless end leakage flow rate $\overline{Q}$ against the phase angles of the surface waviness of both the journal α_1 and the bearing bush α_2 under four cases are shown in Figure 8. It is noted that the variation of $\overline{Q}$ in Figure 8a,c first increased and then decreased with the change of α_2 from 0° to 120°, and it reached its maximum at approximately $\alpha_2 = 60°$, which is consistent with the changing trend of Figure 4b in the case of $n_2 = 3$. At the same time, the variations of $\overline{Q}$ in Figure 8b,d are similar to those of Figure 5b in the case of $n_2 = 6$. The change trends of $\overline{Q}$ are similar to those of $\overline{F}$ in Figure 7, but they are not completely consistency with them. The above phenomenon is probably due to the fact that the value of $\overline{Q}$ was related to the oil pressure and section shape of the gap. The pressure increased with the increase of $\overline{F}$, and the value of $\overline{Q}$ was also increased. Meanwhile, the value of $\overline{Q}$ was also affected by the clearance between the journal and the bearing bush. Therefore, the variations of $\overline{Q}$ were similar to $\overline{F}$, but not in full accord with it.

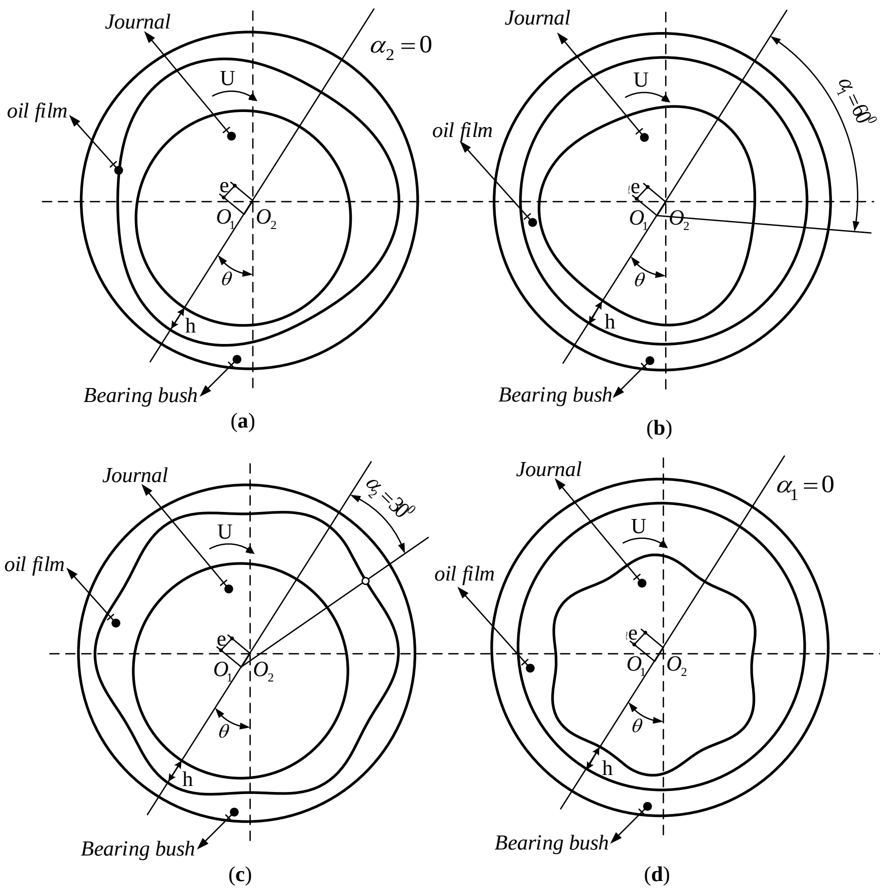

Figure 6. The position of the bearing bush (**a**,**c**) and the journal (**b**,**d**), corresponding to the minimum value of $\overline{F}$.

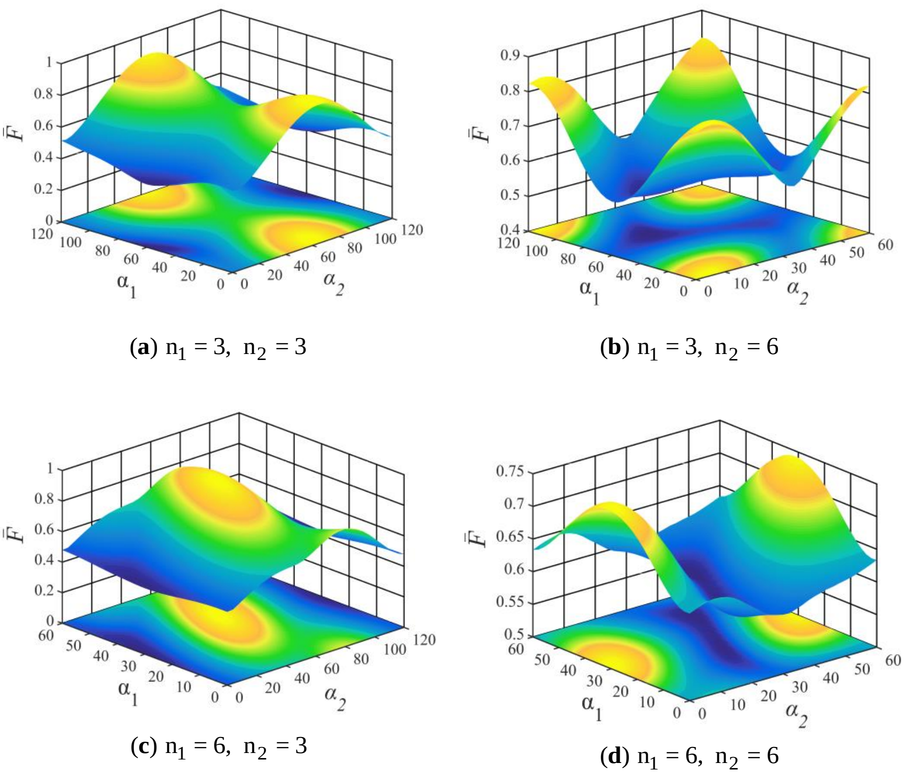

Figure 7. Variations of $\overline{F}$ with the waviness phase angle under four cases.

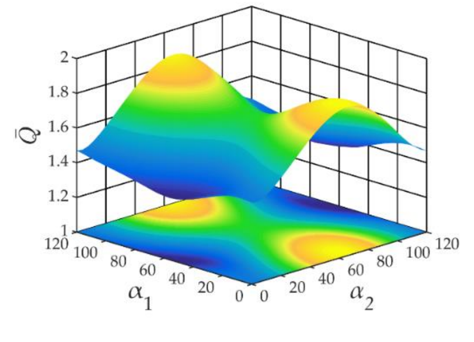

(**a**) $n_1 = 3$, $n_2 = 3$

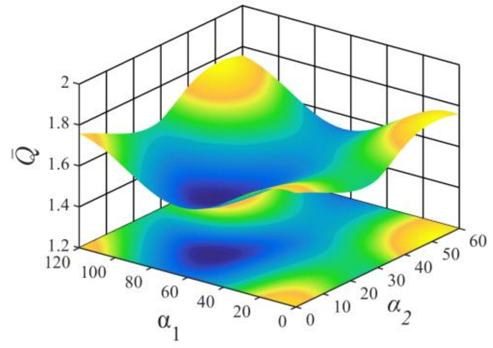

(**b**) $n_1 = 3$, $n_2 = 6$

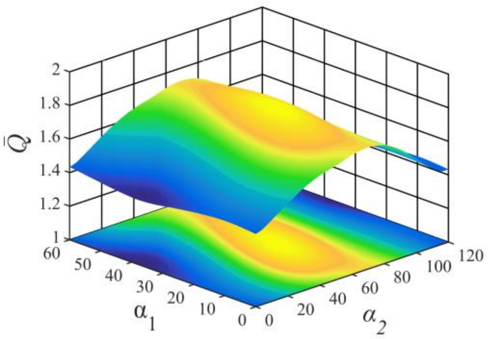

(**c**) $n_1 = 6$, $n_2 = 3$

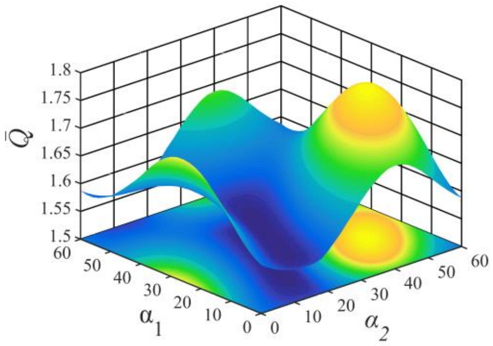

(**d**) $n_1 = 6$, $n_2 = 6$

Figure 8. Variations of $\overline{Q}$ with the wave phase angle under four cases.

4.2.3. Influence on the Friction Coefficient

Figure 9 shows the friction coefficient μ according to different phase angles of the surface waviness on both the journal α_1 and the bearing bush α_2 under four cases. It should be noticed from Figure 9 that the variation of μ is opposite to that of $\overline{F}$ in Figure 7. This is mainly because, with the increase of $\overline{F}$ and the maximum oil pressure increase, the minimum value of the oil film was zero, and therefor the pressure gradient increased. However, the positive value and negative value of the pressure gradient counteracted each other in the integration, and the variation of the friction force was much less than that of $\overline{F}$, as can be observed from Equation (27). According to Equation (28), the change trends of the friction coefficient were opposite to those of $\overline{F}$.

4.2.4. Influence on the Altitude Angle

Figure 10 shows the altitude angle θ against different phase angles of the surface waviness on both the journal α_1 and the bearing bush α_2 under four cases. It is shown that the variation of θ in Figure 10a,c first decreased and then increased with the change of α_2 from 0° to 120° in the case of $n_2 = 3$. In the meantime, the variation in Figure 10b,d first increased and then decreased with the change of α_2 from 0° to 60° in the case of $n_2 = 6$. This is due to the fact that the altitude angle θ was used to adjust the balance of the oil pressure in the X direction, as can be seen in the schematic diagram in Figure 11. The oil film thickness first decreased and then increased in the left-hand load line, and the oil pressure first increased and then decreased when α_2 changed from 0° to 120° in the case of $n_2 = 3$, as can be seen from Figure 6a. Therefore, to keep the balance of the oil force in the X direction, the angle θ needed to first decrease and then increase.

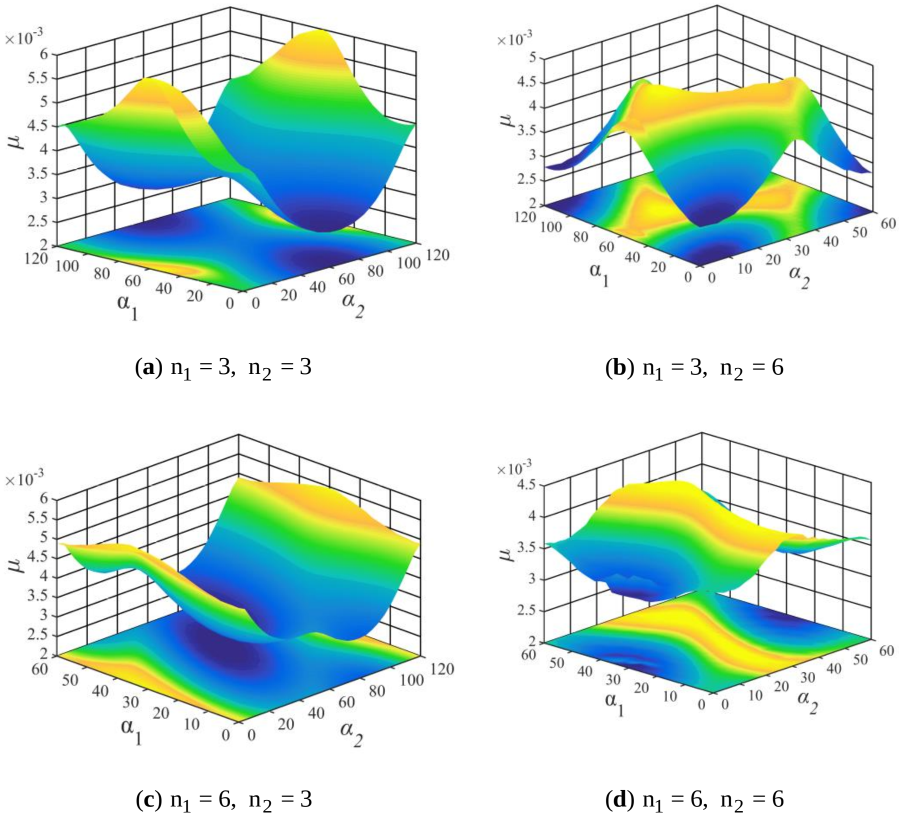

(**a**) $n_1 = 3,\ n_2 = 3$ (**b**) $n_1 = 3,\ n_2 = 6$

(**c**) $n_1 = 6,\ n_2 = 3$ (**d**) $n_1 = 6,\ n_2 = 6$

Figure 9. Variations of μ with the wave phase angle under four cases.

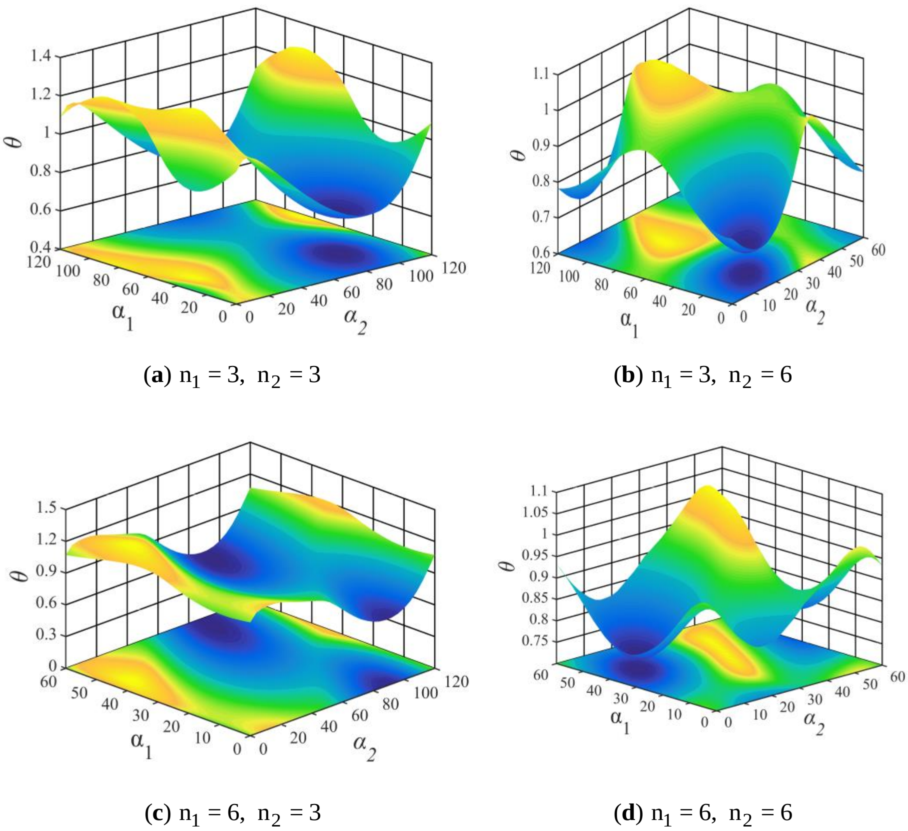

(**a**) $n_1 = 3,\ n_2 = 3$ (**b**) $n_1 = 3,\ n_2 = 6$

(**c**) $n_1 = 6,\ n_2 = 3$ (**d**) $n_1 = 6,\ n_2 = 6$

Figure 10. Variations of θ with the wave phase angle under four cases.

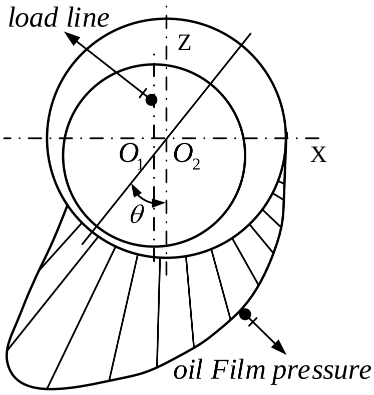

Figure 11. Schematic diagram of the oil pressure without surface waviness.

4.3. Effect of the Waviness Number

Figure 12 shows the bearing dimensionless load capacity $\overline{F}$, dimensionless end leakage flow rate $\overline{Q}$, circumferential friction coefficient μ and altitude angle θ against the eccentricity ratio under the same circumferential waviness amplitude ratio and different waviness numbers. It can be seen that with the decrease of the waviness number, the range of change for $\overline{F}$, $\overline{Q}$, μ and θ became more pronounced. This is mainly due to the fact that the curvature radius of the oil film thickness and the pressure near the attitude angle increased with the decrease of the waviness number. The results of the pressure integration near the maximum value would increase with the reduction of the waviness number, and the results of the pressure integration near the minimum value would decrease with the reduction of the waviness number.

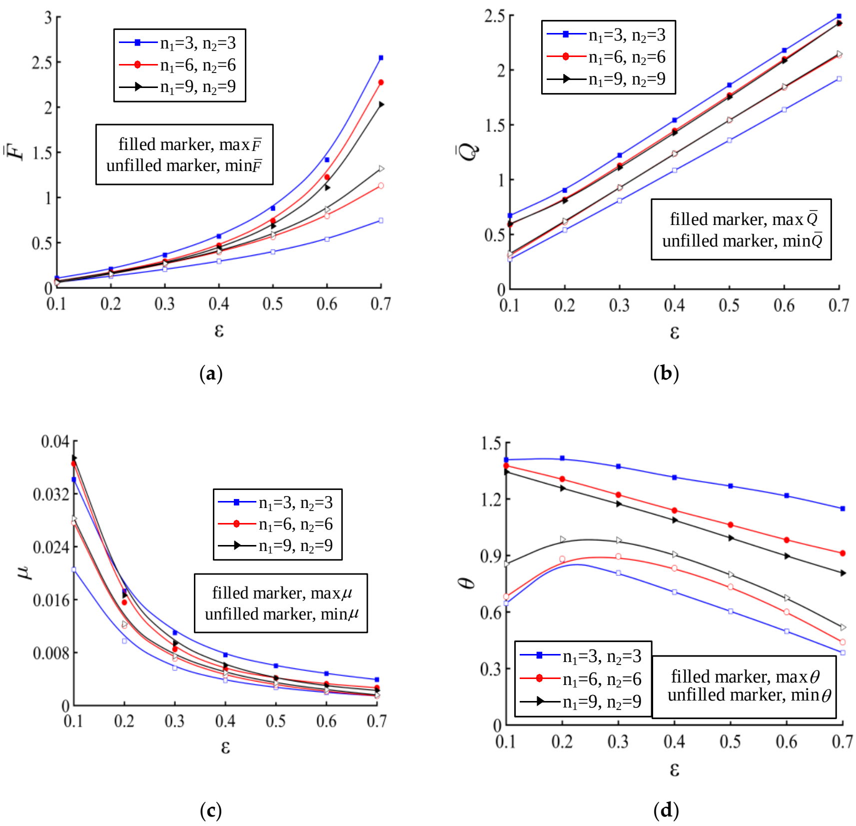

Figure 12. Variations of maximum and minimum dimensionless bearing load capacity (**a**), dimensionless end leakage flow rate (**b**), friction coefficient (**c**) and altitude angle (**d**) with the eccentricity ratio under the same waviness amplitude ratio ($A_1 = 0.05$, $A_2 = 0.1$) and different waviness numbers.

4.4. Effect of the Waviness Amplitude

Figure 13 shows the bearing's static performance against the eccentricity ratio under the same waviness number and different waviness amplitude ratio. The variation tendencies of $\overline{F}$, $\overline{Q}$, μ and θ against the eccentricity ratio were similar to those in Figure 12. As the amplitude ratio increased, the maximum value of $\overline{F}$ increased and the minimum value was basically unchanged. This is because the film thickness reduced with the increase of the waviness amplitude ratio and film pressure increasing. The value of $\overline{F}$ increased with the increasing film pressure. The variation trends of $\overline{F}$, $\overline{Q}$, μ and θ in Figure 13 against the eccentricity ratio was explained in the previous section.

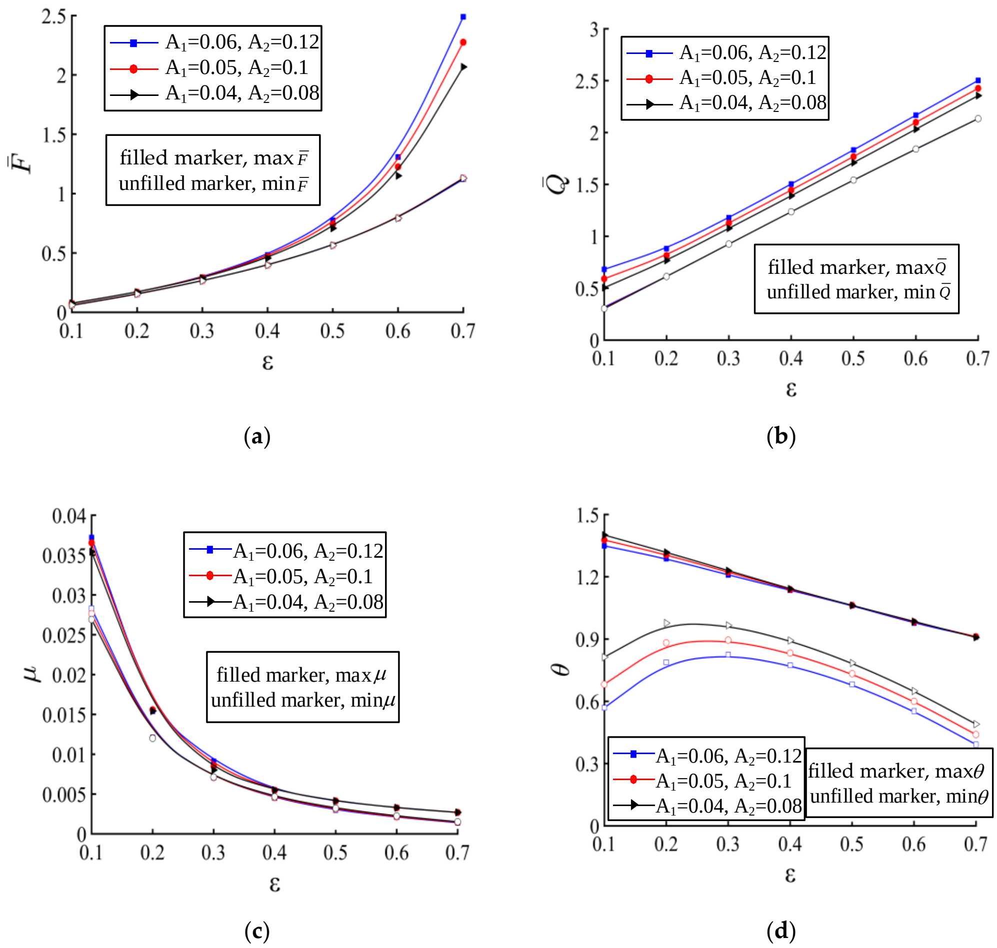

Figure 13. Variations of the maximum and minimum dimensionless bearing load capacity (**a**), dimensionless end leakage flow rate (**b**), friction coefficient (**c**) and altitude angle (**d**) with the eccentricity ratio under the same waviness number ($n_1 = 6$, $n_2 = 6$) and a different waviness amplitude ratio.

5. Conclusions

In the present study, the effect of the surface waviness on the bearing characteristics was investigated. The waviness of the journal and the bearing bush was modeled, and the waviness amplitude, waviness number and phase angles were taken into consideration. From the investigation, several conclusions can be drawn, and they are as follows:

1. Journal bearings with waviness on the bearing bush may deteriorate or enhance the bearing characteristics, depending on the phase angle. A large waviness amplitude and small waviness number can further enhance the bearing characteristics. Such characteristics can be used to design bearings with high performance;

2. In the case of combined or sole presence of surface waviness on the journal or bearing bush, the gap geometry near the attitude angle caused by the waviness of the journal and bearing bush greatly contributes to the pressure generated and hence determines the bearing performance;
3. In the case of combining the journal and bearing bush surface waviness with the growth of the wave number, the maximum values of $\overline{F}$, $\overline{Q}$, μ and θ will decrease while the minimum values will increase, and the bearing characteristics tend to be stable. With the growth of the wave amplitude ratio and the decrease of the wave number, the bearing characteristics will be greatly influenced, and the range of change of $\overline{F}$, $\overline{Q}$, μ and θ becomes larger;
4. The bearing with surface waviness on the journal thus generates periodic variations in its characteristics, due to the alteration of α_1. Regarding the trajectory of the journal's center, it would present periodic motion due to the change in load capacity, which may be a factor that causes a whirling action. As such, when the journal has a small waviness number, the journal's center equilibrium position ($\varepsilon\theta$) generates large periodic variations and damages the bearing's stability. In order to improve the stability of the journal bearing, the waviness amplitude ratio of the journal should be controlled, and a small waviness number should be avoided;
5. The investigation in this paper presents initial research. Subsequent studies will expand on it with other surface irregularities and 3D journal and bearing bush morphologies. The research results indicate that the effect of surface waviness on the bearing system needs further discussion, and the dynamic and transient characteristics should be investigated.

Author Contributions: Conceptualization, M.Y. and X.Z.; methodology, H.L. and X.Z.; writing—original draft preparation, M.Y. and L.B.; writing—review and editing, M.Y. and M.D.; validation and data curation, B.W. and W.W. All authors have read and agreed to the published version of the manuscript.

Funding: This work is supported by the National Natural Science Foundation of China (Grant no. 51675393) and the Fundamental Research Funds for the Central Universities (Grant no. 2019-YB-021).

Institutional Review Board Statement: Not applicable.

Informed Consent Statement: Not applicable.

Data Availability Statement: Data is contained within the article.

Conflicts of Interest: We declare that we do not have any commercial or associative interest that represents a conflict of interest in connection with the work submitted.

Abbreviations

c	the bearing clearance (m)
h	oil film thickness (m)
n	rotational speed (r/min)
p	oil film pressure (N/m)
o_1, o_2	journal and bearing center
η	dynamic viscosity of oil (Ns/m^2)
X, Z	circumferential and axial coordinates
L	axial length of the bearing (m)
D	diameter of the journal (m)
$p_{i,j}$	oil film pressure matrices
$\overline{H}$	dimensionless oil film thickness
k	iteration number
e	eccentricity (m)
r	journal radius (m)
ε	eccentricity ratio (e/c)
θ	attitude angle (rad)

μ	frictional coefficient
ϕ, λ	coordinates ($\phi = X/r, \lambda = 2Z/L$)
U	linear velocity of the journal (m/s)
F_c	frictional force (N)
$H_{i,j}$	oil film thickness matrices
$\overline{F}_x, \overline{F}_z$	load capacity in the X and Z directions
m_1,m_2	grid number in circumferential and axial coordinates
n_1,n_2	waviness numbers of the journal and bearing bush
$A_{m1}A_{m2}$	waviness amplitude of the journal and bearing (m)
$\overline{F}$, F	load capacity ($\overline{F} = 2cF/\eta UrL$)
$\overline{P}$	dimensionless oil film pressure ($pc^2/6U\eta r$)
$\overline{Q}$	dimensionless end leakage flow rate (QL/cUr^2)
ϕ_1,ϕ_2	angles of the start and end of the hydrodynamic film (rad)
$A_{i,j}$,$B_{i,j}$,$C_{i,j}$,$D_{i,j}$,$E_{i,j}$,$F_{i,j}$	coefficient matrices
A_1,A_2	journal and bearing bush surface waviness amplitude ratio ($A_1 = A_{m1}/c, A_2 = A_{m2}/c$)

References

1. Wilson, D. The effect of geometry variations on hydrodynamic bearing performance. *ASLE Trans.* **1966**, *9*, 411–419. [CrossRef]
2. Mokhtar, M.; Aly, W.; Shawki, G. Computer-aided study of journal bearings with undulating surfaces. *ASME J. Tribol.* **1984**, *106*, 468–472. [CrossRef]
3. Mokhtar, M.; Aly, W.; Shawki, G. Experimental study of journal bearings with undulating journal surfaces. *Tribol. Int.* **1984**, *17*, 19–24. [CrossRef]
4. Chennabasavan, T.; Raman, R. The effects of geometric irregularities of journals on the performance of porous bearings. *Proc. Inst. Mech. Eng. Part J J. Eng. Tribol.* **1994**, *208*, 141–145. [CrossRef]
5. Sharma, S.; Rajput, A. Effect of geometric imperfect ions of journal on the performance of micro polar lubricated 4-pocket hybrid journal bearing. *Tribol. Int.* **2013**, *60*, 156–168. [CrossRef]
6. Rajput, A.; Sharma, S. A study of capillary compensated geometrically imperfect six pocket hybrid journal bearing of various geometric shapes of recess. *Proc. Inst. Mech. Eng. Part J J. Eng. Tribol.* **2014**, *228*, 170–186. [CrossRef]
7. Rajput, A.; Sharma, S. Combined influence of geometric imperfections and misalignment of journal on the performance of four pocket hybrid journal bearing. *Tribol. Int.* **2016**, *97*, 59–70. [CrossRef]
8. Rajput, A.; Yadav, S.; Sharma, S. Effect of geometrical irregularities on the performance of a misaligned hybrid journal bearing compensated with membrane restrictor. *Tribol. Int.* **2017**, *115*, 619–627. [CrossRef]
9. Dimofte, F. Wave journal bearing with compressible lubricant–part I: The wave bearing concept and a comparison to the plain circular bearing. *Tribol. Trans.* **1995**, *38*, 153–160. [CrossRef]
10. Dimofte, F. Wave journal bearing with compressible lubricant–part II: A comparison of the wave bearing with a wave-groove bearing and a lobe bearing. *Tribol. Trans.* **1995**, *38*, 364–372. [CrossRef]
11. Lin, T. Steady state performance of finite hydrodynamic journal bearing with three-dimensional irregularities. *Wear* **1994**, *176*, 95–102.
12. Lin, T. The effects of three-dimensional irregularities on the performance characteristics of turbulent journal bearing. *Wear* **1996**, *196*, 126–132. [CrossRef]
13. Van, O.; Beek, A.; Ros, M. A parametric study of the hydro-support. *Tribol. Int.* **2004**, *37*, 617–625.
14. Kwan, Y.; Post, J. A tolerancing procedure for inherently compensated, rectangular aerostatic thrust bearings. *Tribol. Int.* **2000**, *33*, 581–585. [CrossRef]
15. Rahmatabadi, A.; Nekoeimehr, M.; Rashidi, R. Micropolar lubricant effects on the performance of noncircular lobed bearings. *Tribol. Int.* **2010**, *43*, 404–413. [CrossRef]
16. Rasheed, H. Effect of surface waviness on the hydrodynamic lubrication of a plain cylindrical sliding element bearing. *Wear* **1998**, *223*, 1–6. [CrossRef]
17. Pang, X.; Chen, J.; Hussain, S. Study on optimization of the circumferential and axial wavy geometrical conFigureuration of hydrodynamic journal bearing. *J. Mech. Sci. Technol.* **2013**, *27*, 3693–3701. [CrossRef]
18. Wang, X.; Xu, Q.; Wang, B.; Zhang, L.; Yang, H.; Peng, Z. Effect of surface waviness on the static performance of aerostatic journal bearings. *Tribol. Int.* **2016**, *103*, 394–405. [CrossRef]
19. Zmarzły, P. Influence of the internal clearance of ball bearings on the vibration level. *Eng. Mech.* **2018**, *2018*, 961–964.
20. Phalle, V.; Sharma, S.; Jain, S. Influence of wear on the performance of a 2-lobe multirecess hybrid journal bearing system compensated with membrane restrictor. *Tribol. Int.* **2011**, *44*, 380–395. [CrossRef]
21. Sharma, S.; Phalle, V.; Jain, S. Performance of a noncircular 2-lobe multirecess hydrostatic journal bearing with wear. *Ind. Lubr. Tribol.* **2012**, *64*, 171–181. [CrossRef]
22. Sharma, S.; Phalle, V.; Jain, S. Combined influence of wear and misalignment of journal on the performance analysis of three-lobe three-pocket hybrid journal bearing compensated with capillary restrictor. *J. Tribol.* **2012**, *134*, 72–81. [CrossRef]

23. Pawar, S.; Phalle, V. Effect of wear on the performance of hole-entry hybrid conical journal bearing employing constant flow valve compensation. *Proc. Inst. Mech. Eng. Part J J. Eng. Tribol.* **2019**, *233*, 1277–1292. [CrossRef]
24. Li, S.; An, Q. Lubrication performance of planar thrust bearing with consideration of roughness of the surfaces. *Proc. Inst. Mech. Eng. Part J J. Eng. Tribol.* **2018**, *233*, 1046–1058. [CrossRef]
25. Adamczak, S.; Zmarzły, P. Research of the influence of the 2D and 3D surface roughness parameters of bearing raceways on the vibration level. *J. Phys. Conf. Ser.* **2019**, *1183*, 012001. [CrossRef]
26. Li, D.; Yang, X.; Lu, C.; Cheng, J.; Wang, S.; Wang, Y. Tribological characteristics of a cemented carbide friction surface with chevron pattern micro-texture based on different texture density. *Tribol. Int.* **2020**, *142*, 106016.
27. Shen, Z.; Wang, F.; Chen, Z.; Ruan, X.; Zeng, H.; Wang, J.; An, Y.; Fan, X. Numerical simulation of lubrication performance on chevron textured surface under hydrodynamic lubrication. *Tribol. Int.* **2021**, *154*, 106704. [CrossRef]
28. Jain, D.; Sharma, S. Two-lobe geometrically imperfect hybrid journal bearing operating with power law lubricant. *Proc. Inst. Mech. Eng. Part J J. Eng. Tribol.* **2015**, *229*, 30–46. [CrossRef]
29. Jain, D.; Sharma, S. Combined influence of geometric irregularities of journal and turbulence on the performance of four-lobe hybrid journal bearing. *Proc. Inst. Mech. Eng. Part J J. Eng. Tribol.* **2015**, *229*, 1409–1424. [CrossRef]
30. Cui, H.; Wang, Y.; Yue, X. Effects of manufacturing errors on the static characteristics of aerostatic journal bearings with porous restrictor. *Tribol. Int.* **2017**, *115*, 246–260. [CrossRef]
31. Cui, H.; Wang, Y.; Yue, X.; Huang, M.; Wang, W.; Jiang, Z. Numerical analysis and experimental investigation into the effects of manufacturing errors on the running accuracy of the aerostatic porous spindle. *Tribol. Int.* **2018**, *118*, 20–36. [CrossRef]
32. Zoupas, L.; Wodtke, M.; Papadopoulos, C.; Wasilczuk, M. Effect of manufacturing errors of the pad sliding surface on the performance of the hydrodynamic thrust bearing. *Tribol. Int.* **2019**, *134*, 211–220. [CrossRef]
33. Jun, S.; Gui, C. Hydrodynamic lubrication analysis of journal bearing considering misalignment caused by shaft deformation. *Tribol. Int.* **2004**, *37*, 841–848.